Design and Implementation of a Dual Cell Link for Battery-Balancing Auxiliary Power Modules

Weizhong Wang and Matthias Preindl
Department of Electrical Engineering, Columbia University in the City of New York
New York, NY 10027, USA

***Abstract*—In this paper, a novel balancing circuit is proposed for battery-balancing auxiliary power modules. By connecting two battery cells on the primary side instead of filtering capacitors, the topology offers features like reduced-cost and three-mode balancing, including the combination of cell to cell and cell to auxiliary in either power flow direction for each cell within one bridge. A modified phase shift control with asymmetric duty cycle is developed for preventing transformer from saturation, and for adjusting the DC offset current of the transformer to realize different balancing modes. A general design guidance for the passive components of the circuit, such as transformer and output filtering capacitor, is provided for given output power and peak current limitations, inclusive a design example. Three balancing modes are validated at 10 MHz switching frequency.**

I. Introduction

Electrifying conventional vehicles has been prioritized for automotive companies to meet the regulations from US government: double the fuel economy and half the CO2 emissions through 2025. However, the biggest concern that prevents costumers from purchasing electrified vehicles (EVs) is the driving range. EVs with up to 300 miles driving range are not comparable or competitive to gasoline counterparts [1] . Extending the driving range is realized by either new battery material which has higher energy density, or optimally utilizing the battery pack with existing chemistries. The later can be functioned by an on-board battery management system (BMS).

A battery pack consists of several individual cells in series and parallel. Due to many external and internal factors, the battery cells are typically not identical in terms of internal impedance and sensitivity to temperature. This phenomenon has been widely observed in [1]–[5]. These internal and external factors lead to imbalanced batteries during charging and discharging. As a result, only a fraction of battery capacity can be utilized due to voltage protection on the cells, which significantly affects the battery life and utilization of energy. For resolving this issue, battery balancing techniques are needed.

There exist two categories of balancing circuits: passive and active balancing, which are either terminal voltage based or state of charge (SOC) based [6]. However, efficiency is low for passive balancing since there is always energy dissipated. Non-dissipative techniques are preferred in terms of energy efficiency. Redistributive balancing topologies use energy conversion devices to shuttle the excess energy to cells with lower SOC or equally distribute to the stack of battery pack, in our case auxiliary battery [4]. The opposite way is auxiliary to cell (A2C), which requires bidirectional conversion circuits. Step-up converter [7], multi-winding transformer [8], and ramp converter [9] are usually counted as energy conversion based balancing. But they are not cost-friendly in terms of magnetics and parts count [10].

In practice, redistributive balancing is barely implemented in automotive industries due to high cost and complexity [11]. Therefore, how to improve the feasibility of active balancing in terms of size and cost has drawn many researchers' attentions. In EV application, a conversion from high voltage (HV) battery pack (e.g. 400V) to isolated low voltage (LV) loads (e.g. 12V) is known as auxiliary power module (APM). The low voltage loads consist of lighting, wiper, electric compressors, etc. [12], which are at high rated current (e.g. several amperes) but low voltage. For example, Tesla implements an APM with a rated power of 2.4 KW (200 A at 12 V) in its Model S.

Based on the concept of APM, one attempt of reducing cost to balancing circuit is to integrate balancing functionality into the APM by replacing high step-down DC-DC converter with individual converters with low power rating. The dual active bridge (DAB) converter is chosen as DC-DC converter between high voltage (HV) cells to low voltage (LV) battery stack in [11]. But eight power switches per DAB are over-cost if better switches are used for better performance, e.g. SiC MOSFETs.

For further reducing the cost of balancing circuits without sacrificing power level or balancing functions, this paper proposes a DC-DC converter topology that reduces the number of necessary power switches. Meanwhile, a direct C2C balancing mode can be achieved without any external circuits. The paper is organized as follows: the topology is explained in Section II, including the proposed asymmetric control and operation modes. In Section III, the output power equations are derived in steady state as well as the realization of the proposed three operation modes. A general design guidance is given in Section IV based on derived ZVS range and power/current requirements. The simulation validation is performed in Section V. Lastly, the paper is concluded in Section VI.

II. Proposed APM with Built-in Active Balancing

A diagram of an APM with individual DC-DC converters is depicted in Fig. 1. Output voltage of each DC-DC converter is regulated to LV range (e.g. 11 - 16 V). The current drawn from each converter (battery cell) is controlled to balance the HV battery pack and to meet the load current requirements at the same time. The topology that is applied in the converter block is shown in Fig. 2.

978-1-5386-3048-8/18/$31.00 ©2018 IEEE

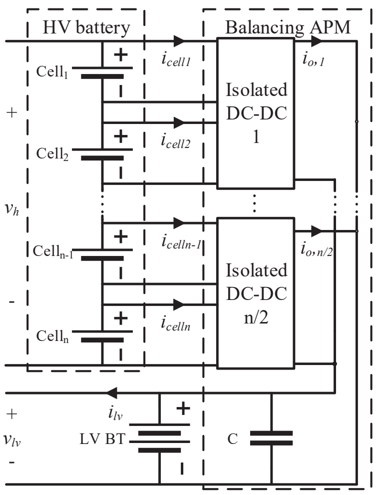

Fig. 1. The realization of APU balancing

Half bridge and full bridge (HFB) are combined on the primary and secondary sides via a high frequency transformer. The traditional filtering capacitors on the primary side are replaced by two battery cells. The control algorithms of DAB have been heavily investigated, such as PWM modulation and phase shifted control. The same algorithms can be applied because of the similarity between DAB and HFB.

However, due to the unbalanced half-bridge voltages, traditional 'symmetric' phase shift control cannot operate stably. Symmetric means that switches on primary side and secondary side are turned on for the same length of time but in a complementary fashion, e.g. 50% duty cycle. Some modifications must be made to apply the phase shift control.

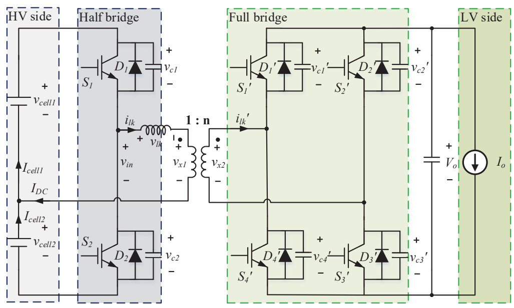

Fig. 2. The HFB topology applied in APU

A. Asymmetric Duty Cycle

When the cells are unbalanced in one HFB device, the leakage inductor current tends to drain more energy from the cell with higher voltage, because of the steeper slope generated by the inductor voltage, i.e. v_{lk} in Fig. 3. If without control, the HFB topology inherently balances out the attached two cells, but in a destructive fashion with the sacrifice of efficiency due to drifting phenomenon. So called flux walking due to the unbalanced current of leakage inductor eventually

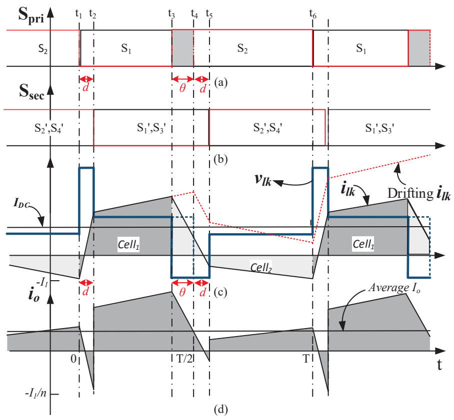

Fig. 3. The waveforms of operating half-full bridge converter without asymmetric control (red dotted line), and with asymmetric control (black solid line)

leads to transformer saturation, as shown by red dotted line in Fig. 3 (c). However, it can be turned into a good feature for battery balancing application by some proper control schemes — asymmetric control.

By introducing an adjustment of duty cycle θ, forcing $\Delta i_{lk} = 0$ within one time period T prevents transformer from infinitely increasing DC offset current unless two cells are balanced. The DC offset current is defined as the average current for the leakage inductance of the transformer, as shown in Fig. 3. The parameter θ is derived based on the boundary condition $\Delta i_{lk} = 0$, shown as follows:

$$\theta = \frac{T}{2}\frac{V_{cell1} - V_{cell2}}{V_{cell1} + V_{cell2}} = \frac{T}{2}\frac{\Delta V}{V_{DC}} \tag{1}$$

where, the cells' voltages v_{cell1} and v_{cell2} are approximated as constant V_{cell1} and V_{cell2} due to their slower variation at high frequency, e.g. 10 MHz. It can be also known that the waveform of leakage inductance current ilk is the superposition of two cells currents when they are alternatively conducting, i.e. one is conducting and the other is not, as shown in Fig. 3 by the dark and light shaded area. The average current from cell 1 is represented as I_{cell1}, and I_{cell2} for cell 2.

It can be seen from (1) that the duty cycle adjustment θ is only a function of the voltage difference and summation of the two cells in one HFB. Note that the phase shift d is set to be the same for both S_1 and S_2.

B. Feasible Operating Modes

For balancing the battery pack, the proposed HFB topology can operate in three typical modes with proper DC offset current: a) *C2C* and *cell to auxiliary (C2A)*: high-SOC cell charges LV battery and low-SOC cell in the same branch, b) *C2C* and *Auxiliary to cell (A2C)*: high-SOC cell and LV battery charge the low-SOC cell, c) *C2A only*: high-SOC cell and low-SOC cell charge the LV battery with either same or different current levels based on the initial SOC bias between them.

1) C2C and C2A: In this mode, the high-SOC cell is demanded to supply energy to low-SOC cell and auxiliary power supply. It is suitable for the cases where the LV battery is charging and initial SOC bias is significant. This process is dissipating energy from high-SOC cell and partially charging low-SOC cell. Meanwhile, the LV battery is charging by the rest of energy from high-SOC cell. This mode can be realized by setting i) positive average current ($I_{cell1} > 0$) for high-SOC cell, ii) negative average current ($I_{cell2} < 0$ and $I_o < 0$) for low-SOC cell and LV battery.

2) C2C and A2C: This mode is triggered when HV battery side is charging as well as the presence of significant difference between the SOCs of two cells in one branch. LV battery and high-SOC cell merge their energy to low-SOC cell. As a result, the bias among HV battery cells is eliminated faster than the A2C-only techniques. The required polarities of I_{cell1}, I_{cell2} and I_o are positive, negative and positive, respectively.

3) C2A-Only: When both cells in one HFB are 'stronger' compared with other cells on the HV side, it is more suitable to discharge both cells simultaneously but in different C-rates . Therefore, the initial SOC bias is gradually eliminated due to the C-rate difference while charging LV battery. The control unit forces positive power demands for the both cells ($I_{cell1}\&I_{cell2} > 0$) to LV side ($I_o < 0$).

Note that all the modes can be modified to the inversed power flow direction without changing the control scheme but the phase shift d as the same with traditional DAB.

C. Corresponding Realization of Modes 1, 2 and 3

It can be seen from the Fig. 3 that DC current offset $I_{DC} = I_{cell1} - I_{cell2}$. As long as $I_{DC} > 0$, i.e. $I_{cell1} > I_{cell2}$, cell 1 offers more energy, and vice versa. For example, if $I_{DC} = 10A$, it indicates that cell 1 supplies 10 A more current than cell 2. When $I_{DC} > I_{cell1}$, $I_{cell2} < 0$ will be observed. As a result, cell 1 is discharging while cell 2 is charging, despite that LV side is charging or not.Therefore, the DC current offset gives an idea of balancing direction and speed, which will be explicitly controlled in the battery balancing algorithm.

Given the discussion above, mode 1 requires that cell 1 supplies the energy (positive I_{cell1}) and cell 2 absorbs the partial energy (negative I_{cell2}) dissipated by cell 1. It is feasible when $I_{DC} > I_{cell1} > 0$. In this case, I_{cell1} is definitely positive due to C2A direction of power flow.

Mode 2 requires A2C power flow direction. Except for the A2C power flow, mode 2 is similar with mode 1 in terms of the reaction of cell 2. The direction of A2C power flow is the result of negative phase shift d. The I_{DC} boundary conditions for this mode preserve as mode 1.

The negative I_{cell2} is not valid in mode 3 anymore. Conversely, energy is needed from cell 2. Therefore, the condition is changed to $I_{cell1} > I_{DC} > 0$ so that cell 2 outputs power instead of gaining power. The other requirements for cell 1 and direction of power flow remain the same as mode 1. The modes discussed above are summarized in Table I.

TABLE I
FEASIBLE BALANCING MODES AND CORRESPONDING POWER FLOW

Conditions	Charging	Discharging
$I_{DC} > I_{cell1} > 0$ ($d > 0$)	Cell 2 and LV	Cell 1
$I_{DC} > I_{cell1} > 0$ ($d < 0$)	Cell 2	Cell 1 and LV
$I_{cell1} > I_{DC} > 0$ ($d > 0$)	LV	Cell 1 and Cell 2

III. OUTPUT CHARACTERIZATION

A. Output Power in Steady State for Balanced Cells

If the two cells in one HFB are balanced, i.e. same SOC/voltage, a constant level of output current/power is required. This bridge is not operating under balancing modes. Instead, a pure-power-deliver mode is engaged. That is, the bridge is only a media of transferring energy from two cells to the auxiliary without balancing functionality, and vice versa.

For the balanced cells, θ is naturally set to zero and $V_{cell1} = V_{cell2} = V_{cell}$. Therefore, the delivered power is simplified to the following expression, as derived in DAB applications [13], [14]:

$$P_o = V_o I_o = \frac{2V_o}{T}\int_0^{\frac{T}{2}} i_o(t)dt = \frac{TV_oV_{cell}}{2nL_{lk}}(1-d')d' \quad (2)$$

where, n is the turns ratio of the transformer. d' is the normalized phase shift, i.e. $d' = d/\frac{T}{2}$. Assuming that output current I_o and voltage V_o are constant, P_o can be controlled by the phase shift d' based on the equation above. It can be seen that there is no output power when phase shift is zero.

B. Output Power in Steady State for Unbalanced Cells

The enlarged waveform of leakage inductor current is depicted in Fig. 4 to obtain the output power and DC current offset in steady state. Firstly, the current drawn by cell 1 is highlighted in dark gray as well as cell 2 in light gray. The averaged cell currents can be geometrically extracted

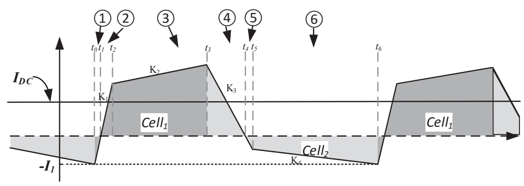

Fig. 4. The enlarged waveform of leakage inductor current

by the shaded area divided by the entire time period. The repeated waveform is divided into six parts, denoted from 1 - 6. Therefore, averaged cell 1 current:

$$I_{cell1} = -A_1 + A_2 + A_3 \quad (3)$$

where, A stands for the area of corresponding part from 1 to 6. Equation (3) can be expressed with the geometric property of the waveform, thus

$$\begin{aligned} I_{cell1} = &-\frac{I_1}{2}\times t_1 + \frac{(t_2-t_1)(-I_1+K_1t_2)}{2} \\ &+ \frac{[2(-I_1+K_1t_2)+K_2(t_3-t_2)](t_3-t_2)}{2} \end{aligned} \quad (4)$$

Similarly, I_{cell2} can be obtained:

$$
\begin{aligned}
I_{cell2} &= -(A_4 - A_5 - A_6) \\
&= -(\frac{(t_4-t_3)[(-I_1+K_1t_2)+K_2(t_3-t_2)]}{2} \\
&\quad - \frac{(t_5-t_4)^2K_3}{2} + \\
&\quad \frac{[2(t_5-t_4)K_3+(t_6-t_5)K_4](t_6-t_5)}{2})
\end{aligned} \tag{5}
$$

where,

$$
\begin{aligned}
K_1 = V_{c1}(t) + V_o(t)/n, K_2 = V_{c1}(t) - V_o(t)/n, \\
K_3 = V_{c2}(t) + V_o(t)/n, , K_4 = V_{c2}(t) - V_o(t)/n. \\
t_1 = I_1/K_1, \quad t_2 = d, \quad t_3 = T/2 - \theta, \\
t_4 = (-I_1 + K_1t_2 + K_2(t_3 - t_2))/K_3 + t_3, \\
t_5 = T/2 + d, \quad t_6 = T
\end{aligned} \tag{6}
$$

Given the waveform of the output current as shown in Fig. 3 (d), the similar analysis can be made as (3) and (5). Average output power can be obtained as follows:

$$
\begin{aligned}
P_o = V_oI_o &= \frac{V_o}{T}\int_0^T i_o(t)dt \\
&= \frac{V_oT}{8L_{lk}n}[V_{cell1}\alpha_1 + V_{cell2}\alpha_2]
\end{aligned} \tag{7}
$$

and

$$
\begin{aligned}
\alpha_1 &= -1 + 4d' + 4\theta' - 2d'^2 - 4\theta'^2 - 8d'\theta' \\
\alpha_2 &= 1 + 4\theta' - 2d'^2 - 4\theta'^2 - 8d'\theta'
\end{aligned} \tag{8}
$$

where, θ' is the normalized value for cleaner expression, i.e. $\theta' = \theta/\frac{T}{2}$. It can be verified that the output power has the same expression as (7) when the cells are balanced ($V_{cell1} = V_{cell2}$, $\theta = 0$). So, equation (2) can be included as a special case for (7). Therefore, the general form of the output power for HFB topology can be summarized as (7) and (8). These equations will be used to help the circuit design in Section IV.

IV. Design Guidance

A. Range of Zero Voltage Switching

It is well-know that DAB is a bi-directional DC-DC converter with zero voltage switching (ZVS) to reduce the switching loss when switching frequency is high, e.g. 10 MHz. As a derivative of DAB, the proposed HFB is also capable of ZVS by appropriately exciting the switches. The ZVS conditions that need to be satisfied can be summarized as follows:
1. At the instant when switches are turned on, its anti-body diode is conducting.
2. At the instant when the switches are turned off, the current flow through them is positive.

They are interpreted into:

$$
\begin{aligned}
i_{lk}(t_2) > i_{com}, i_{lk}(t_3) > i_{com}, \\
i_{lk}(t_5) < -ni_{com}, i_{lk}(t_6) < -ni_{com}
\end{aligned} \tag{9}
$$

where, i_{com} is the commutating current that the parasitic capacitor needs to be fully discharged. So that the corresponding switch can be turned on while its anti-body diode is conducting. The parameter i_{com} is usually obtained from the manufacturers of the power switches.

If i_{com} is assumed to be significantly smaller than operating current, which is the case for small parasitic capacitors, one can say $i_{com} \approxeq 0$. Additionally, $K_2 > 0$ and $K_4 < 0$ are valid as long as $v_{cell} > v_o/n$ in a specific design. Therefore, ZVS conditions (9) are simplified to: $i_{lk}(t_2) > 0$ and $i_{lk}(t_5) < 0$. The upper bound of the inductor current is limited by $i_{lk}(t_2) > 0$. Similarly, lower bound is determined by $i_{lk}(t_5) < 0$. The two extreme operating conditions are highlighted by red and green circles shown in Fig. 5. Therefore, the ZVS range based on initial condition of inductor current within each period is derived as:

$$
0 < \frac{nV_{cell2} - V_o}{nL_{lk}}\frac{(1-d')T}{2} \leq I_1 \leq \frac{nV_{cell1} + V_o}{nL_{lk}}\frac{dT}{2} \tag{10}
$$

Alternatively,

$$
\begin{aligned}
&\frac{T}{8L_{lk}}[(3 - 4\theta' - 4\theta'^2)V_{cell1} - \\
&\qquad (5 - 4d' + 4\theta' + 4\theta'^2)V_{cell2} + 2V_x] \\
&\qquad < I_{DC} < \\
&\frac{T}{8L_{lk}}[(3 - 4d' - 4\theta' - 4\theta'^2)V_{cell1} - \\
&\qquad (1 + 4\theta' + 4\theta'^2)V_{cell2} + 8d'V_x]
\end{aligned} \tag{11}
$$

where, V_x is primary-side referred output voltage $V_x = V_o/n$. Both current inequalities are related to the design parameters (e.g. T and L), duty cycle adjustment θ, and phase shift d. However, θ is constant within one period by assuming the cell voltages vary slowly compared with switching frequency. Therefore, the amplitude of the both currents in (10) and (11) can be controlled within a range where $0 < d' < 1 - 2\theta'$.

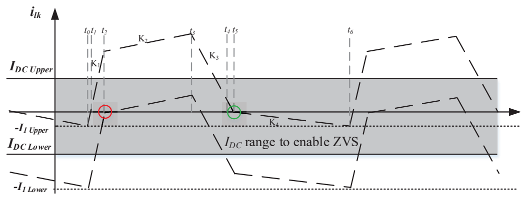

Fig. 5. The range of I_{DC} to ensure ZVS operation

B. Selection of Leakage Inductance

1) Power limitation: The rated output power per HFB should be considered for transformer design. Based on (7), the conditions that physically/electrically limit the output power are switching frequency T, leakage inductance L, and turns ratio n. On the other hand, the range of phase shift d and the duty cycle adjustment θ are the controllable variables that tune the output power within the physical/electrical range.

Based on (7), the power spectrum can be obtained by sweeping phase shifts d and the leakage inductance levels L_{lk} under the worst scenario of V_{cell1} and V_{cell2}. In this study, the power requirement is asked to achieve under worst case, but the requirements could be loosed in other balancing-oriented designs. The worst case is defined when both cells are approaching fully discharged, e.g. cut-off voltage. So the range of leakage inductance is narrowed down to guarantee constant power in the worst case scenario. A design example will be given later for a better explanation.

2) Peak current limitation (instantaneous): Additionally, the maximum discharge current is normally bounded to prevent the cells being destroyed permanently. Therefore, the unlimited cell current level is not desired. By combining (3) and (10) when $i(t_5) = 0$ (green circle in Fig. 5), the current of cell 1 can be derived as:

$$I_{cell1}^{peak} = \frac{T}{2L_{lk}}[(1-2\theta')V_{cell1} \\ -(1-d')V_{cell2}+(d'+2\theta')V_x] \tag{12}$$

The current I_{cell1}^{peak} is the peak current for the HFB, which can be explained by i) I_{cell1} is needed to be high enough to provide a constant output power and charge cell 2, simultaneously, ii) I_{cell1} cannot exceed I_{cell1}^{peak} to ensure ZVS. Naturally, I_{cell1}^{peak} is the maximum achievable value without sacrificing output power and ZVS conditions. The worst case scenario is reached when $V_{cell1} = V_{max}$ and $V_{cell2} = V_{min}$, since K_1 and K_2 are largest as well as the energy needed from cell 2. In equation (12), d' is given when required output power is known, and V_{cell1} and V_{cell2} are fixed. Therefore, peak current can be regulated by properly designing leakage inductance at operating switching frequency.

C. Design Example

In this study the constant output power is selected as 40 W to LV battery. It is designed to be higher than the rated output power (12 W per cell for 1.2 KW system) from a classic APM [15]. The turns ratio is chosen as 1:5 for the reason that $K_2 > 0$ and $K_4 < 0$, as discussed in the previous section.

Given the power and peak current limitations, the power spectrum for the worst case is illustrated in Fig. 6(a) as well as the peak current distribution in Fig. 6(b). Inductance values from 1.7 nH to 2 nH are swept to pick the proper design of the leakage inductance. It can be observed that the power requirement can be achieved in each condition by tuning d. For smaller peak current, $L = 2$ nH is picked in this design. It shows 30 and 48 A peak currents with 24 and 40 W output power.

Note that the design is based on extreme conditions. In practice, the cells are not asked for energy if they are empty. So the design restrictions could be loosed for more realistic designs based on this guidance. In other words, the peak current will be much less in realistic operation points. However, for showing the full capability, the extreme conditions are considered in this study. The transformer design procedure is summarized in a flowchart as shown in Fig. 7.

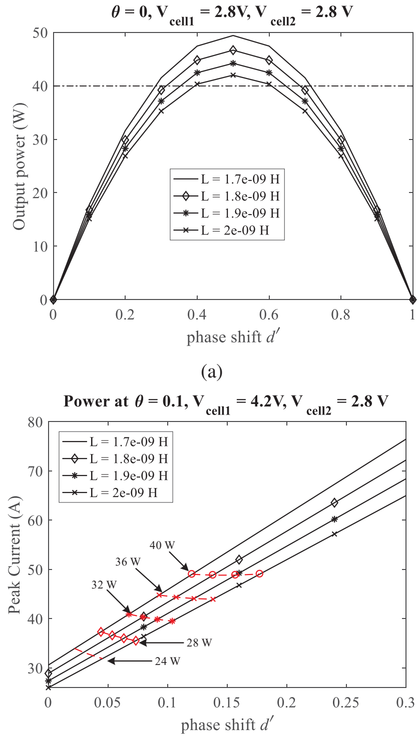

(a)

(b)

Fig. 6. (a) selections of leakaged inductant for constant power requirement , (b) Equi power lines (red) vs. peak current (black) from one cell

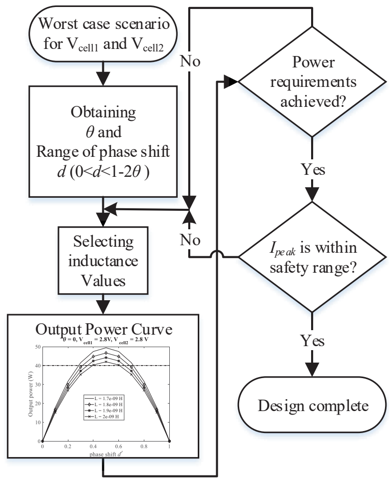

Fig. 7. Flow chart of the design guidance

TABLE II
PARAMETERS IN SIMULATION

Parameters	Leakage Inductance (nH)	Turns Ratio	Switching Frequency (MHz)
Values	2	1:5	10

V. RESULTS

Three potential operating conditions are simulated and illustrated in Fig. 8(a) - Fig. 8(c). The leakage inductance is set to 2 nH, based on the analysis previously. The complete list of the simulation parameters is summarized in Table II.

Each operating condition is required to offer 40 W average output power. Given cell voltages, the duty cycle adjustment θ and phase shift d are obtained from (1) and (7). Fig. 8(a) shows that the HFB is operating under pure-power-deliver mode, i.e.

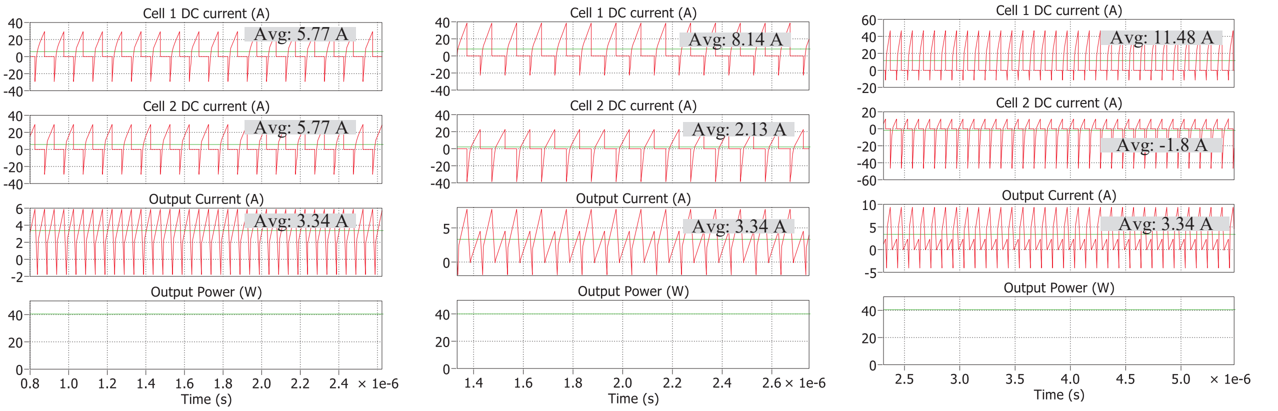

(a) (b) (c)

Fig. 8. (a) C2A: Balanced cells (3.5 V), (b) C2A: Unbalanced cells (4 V and 3.5 V), and (c) C2A and C2C: Unbalanced cells (4 V and 3 V): with 40 W constant output power, average value (green) and instantaneous value (red)

balanced cells. Cell 1 and cell 2 generate average 5.77 A constant current. Averaged output current is 3.34 A, which leads to 40 W output power with 12 V nominal output voltage.

Fig. 8(b) shows unbalanced cells case, which simulates the mode 3 (C2A-only). It shows that the distribution of two cells' current differs due to the DC offset current, $I_{DC} = 10.27A$. The cell with higher voltage (cell 1) produces average 8.14 A current, while cell 2 offers less current, 2.13 A. Please note that the cell currents are arbitrary, they can be controlled by I_{DC} with proper balancing algorithm.

In Fig. 8(c), mode 2 (C2C and C2A) is achieved by simply adjusting θ to make the I_{DC} locate to the desired range ($I_{DC} > I_{cell1} > 0$). As discussed previously, I_{DC} enables negative current flow to one cell even with another cell powering stack. It can be seen from Fig. 8(c) that cell 1 has positive power flow while cell 2 has negative power flow, which accelerates balancing when the two cells suffer large imbalance.

VI. Conclusions

The paper proposes a new balancing circuit with three typical operating modes. By integrating APM, it can significantly reduce the cost of active balancing circuit. Furthermore, only one HFB device is needed for balancing two cells, which leads to less switch components compared with other balancing topologies. Asymmetric control and transformer DC current offset are introduced to i) keep VA balance of leakage inductance and, ii) offer flexibility of transferring energy from cell to auxiliary while charging the low voltage cell, simultaneously. This function cannot be achieved by other topologies, such as fly-back and DAB, because the energy has to pass through the LV auxiliary battery in order to move energy from one cell to another. The design guidance is given to select the leakage inductance and turns ratio without sacrificing the output power. ZVS range is determined by the DC offset current, which outlines the peak current limitation for the cells. A verification simulation is performed to validate the theory of the proposed topology with constant output power requirement.

References

[1] J. Cao and A. Emadi, “Batteries need electronics,” *Industrial Electronics Magazine, IEEE*, vol. 5, no. 1, pp. 27–35, 2011.
[2] A. A. Hussein, “Experimental modeling and analysis of lithium-ion battery temperature dependence,” *2015 IEEE Applied Power Electronics Conference and Exposition (APEC)*, pp. 1084–1088, 2015.
[3] D. Andre, M. Meiler, K. Steiner, H. Walz, T. Soczka-Guth, and D. U. Sauer, “Characterization of high-power lithium-ion batteries by electrochemical impedance spectroscopy. II: Modelling,” *Journal of Power Sources*, vol. 196, no. 12, pp. 5349–5356, 2011.
[4] L. McCurlie, M. Preindl, P. Malysz, and A. Emadi, “Simplified control for redistributive balancing systems using bidirectional flyback converters,” *2015 IEEE Transportation Electrification Conference and Expo, ITEC 2015*, 2015.
[5] M. Preindl, C. Danielson, and F. Borrelli, “Performance evaluation of battery balancing hardware,” in *Control Conference (ECC), 2013 European*. IEEE, 2013, pp. 4065–4070.
[6] J. Cao, N. Schofield, and A. Emadi, “Battery balancing methods: A comprehensive review,” in *Vehicle Power and Propulsion Conference, 2008. VPPC '08. IEEE*. IEEE, 2008, pp. 1–6.
[7] S. T. Hung, D. C. Hopkins, and C. R. Mosling, “Extension of Battery Life via Charge Equalization Control,” *IEEE Transactions on Industrial Electronics*, vol. 40, no. 1, pp. 96–104, 1993.
[8] S. Li, C. C. Mi, and M. Zhang, “A high-efficiency active battery-balancing circuit using multiwinding transformer,” *IEEE Transactions on Industry Applications*, vol. 49, no. 1, pp. 198–207, 2013.
[9] M. Tang and T. Stuart, “Selective buck-boost equalizer for series battery packs,” *IEEE Transactions on Aerospace and Electronic Systems*, vol. 36, no. 1, pp. 201–211, 2000.
[10] S. W. Moore and P. J. Schneider, “A Review of Cell Equalization Methods for Lithium Ion and Lithium Polymer Battery Systems,” in *SAE World Congress*, mar 2001, pp. 1–7.
[11] M. Evzelman, M. M. Ur Rehman, K. Hathaway, R. Zane, D. Costinett, and D. Maksimovic, “Active Balancing System for Electric Vehicles With Incorporated Low-Voltage Bus,” *IEEE Transactions on Power Electronics*, vol. 31, no. 11, pp. 7887–7895, nov 2016.
[12] R. Hou, P. Magne, B. Bilgin, and A. Emadi, “A topological evaluation of isolated DC/DC converters for Auxiliary Power Modules in Electrified Vehicle applications,” *Conference Proceedings - IEEE Applied Power Electronics Conference and Exposition - APEC*, vol. 2015-May, no. May, pp. 1360–1366, 2015.
[13] R. T. Naayagi, A. J. Forsyth, and R. Shuttleworth, “High-power bidirectional DC-DC converter for aerospace applications,” *IEEE Transactions on Power Electronics*, vol. 27, no. 11, pp. 4366–4379, 2012.
[14] A. Rodríguez, A. Vázquez, D. G. Lamar, M. M. Hernando, and J. Sebastián, “Different purpose design strategies and techniques to improve the performance of a dual active bridge with phase-shift control,” *IEEE Transactions on Power Electronics*, vol. 30, no. 2, pp. 790–804, 2015.
[15] R. Hou and A. Emadi, “Applied Integrated Active Filter Auxiliary Power Module for Electrified Vehicles with Single-Phase Onboard Chargers,” *IEEE Transactions on Power Electronics*, vol. pp, no. 99, pp. 1–1, 2016.